JTTEE5 15:387-399
DOI: 10.1361/105996306X124392
1059-9630/$19.00 © ASM International

Hot Corrosion Resistance of High-Velocity Oxyfuel Sprayed Coatings on a Nickel-Base Superalloy in Molten Salt Environment

T.S. Sidhu, S. Prakash, and R.D. Agrawal

(Submitted July 8, 2005; in revised form January 24, 2006)

No alloy is immune to hot corrosion attack indefinitely. Coatings can extend the lives of substrate materials used at higher temperatures in corrosive environments by forming protective oxides layers that are reasonably effective for long-term applications. This article is concerned with studying the performance of high-velocity oxyfuel (HVOF) sprayed NiCrBSi, Cr_3C_2-NiCr, Ni-20Cr, and Stellite-6 coatings on a nickel-base superalloy at 900 °C in the molten salt (Na_2SO_4-60%V_2O_5) environment under cyclic oxidation conditions. The thermogravimetric technique was used to establish kinetics of corrosion. Optical microscope, x-ray diffraction, scanning electron microscopy/electron dispersive analysis by x-ray (SEM/EDAX), and electron probe microanalysis (EPMA) techniques were used to characterize the as-sprayed coatings and corrosion products. The bare superalloy suffered somewhat accelerated corrosion in the given environmental conditions, whereas hot corrosion resistance of all the coated superalloys was found to be better. Among the coatings studied, Ni-20Cr coated superalloy imparted maximum hot corrosion resistance, whereas Stellite-6 coated indicated minimum resistance. The hot corrosion resistance of all the coatings may be attributed to the formation of oxides and spinels of nickel, chromium, or cobalt.

Keywords high-velocity oxyfuel process, hot corrosion, protective coatings, superalloy

1. Introduction

Advances in materials development and cooling schemes will lead to increased operation temperatures of gas turbines, boilers, and industrial waste incinerators. The combination of such high temperatures with contaminants of environment and low-grade fuels, such as sodium, sulfur, vanadium, and chlorine, require special attentions to the phenomenon of hot corrosion, which is one of the main failure modes of hot section components in gas turbines. Superalloys have been developed for high-temperature applications, but they are not able to meet both the high-temperature strength and the high-temperature corrosion resistance simultaneously, so protective coatings on superalloys are used to counter the latter (Ref 1).

Coatings extend the lives of the materials by allowing mechanical properties of the substrate materials to be maintained while protecting them against wear or corrosion (Ref 2). The coatings should possess the required mechanical properties, adhesion, and metallurgical stability in contact with the substrate. Porosity, oxide stringers and clusters, fissures, and cracks may open corrosion paths through the coating to the substrate. Therefore, it is important to obtain coatings with both low porosity and low oxide content to provide optimum protection against hot corrosion and oxidation (Ref 3).

Coatings can be deposited by thermal spraying (flame spraying, vacuum plasma spray [VPS], low-pressure plasma spray [LPPS], high-velocity oxyfuel [HVOF]), by sputtering, or by evaporation; however, generally, for industrial applications, thermally sprayed coatings are preferred (Ref 4).

Among the thermal spraying processes, HVOF is most popular and has been widely adopted by many industries due to its flexibility, cost effectiveness, and the superior quality of coatings produced. High-velocity oxyfuel is a relatively new thermal spray process (the Sulzer Metco Diamond Jet HVOF was developed in 1988) offering coatings with higher bond strengths and hardness together with lower porosity, compared with its other thermal spray counterparts (Ref 5). High-velocity oxyfuel coatings are being studied extensively for their corrosion-resistant properties (Ref 6). So far, several HVOF spraying coatings have been subjected to the corrosion test in seawater. In addition to the cermets (Ref 7-9), the anticorrosion alloys (Ref 10-12) were adopted as the coating materials. These studies concluded that the HVOF method is superior to other spraying techniques for developing coatings having higher corrosion resistance. The HVOF coatings are widely used in various engineering components for imparting wear and corrosion resistance including propellers, pump impellers and casings, superheaters and preheaters of boilers, valve bodies/trim, and pipe systems (Ref 13). Therefore, in this study, the HVOF process has been selected to deposit the selected coatings.

T.S. Sidhu, S. Prakash, and **R.D. Agrawal,** Metallurgical & Materials Engineering Department, Indian Institute of Technology Roorkee, Roorkee-247 667, India. Contact e-mail: tssidhu@rediffmail.com.

The composition and structure of the coatings are determined by the role that they have to play in the various material systems and performance environments (Ref 14). The coating should have a composition that will react with the environment to produce the most protective scale possible, provide corrosion resistance with long-term stability, and have resistance to cracking or spallation under mechanical and thermal stresses induced during operation of the components (Ref 15). In the service environment, the protective oxide scale should not react with the corrosive environment, and at the same time it should not allow the corrosive species to diffuse through the coating.

There is an increasing interest in the deposition of nickel-base metallic alloys for protection against corrosion. Nickel-chromium (Ni-Cr) alloys have been used as coatings to deal with oxidation and corrosive environments at high temperature. When Ni is alloyed with Cr, this element oxidizes to protective surface oxide Cr_2O_3 at rates that could make it suitable for use up to about 1200 °C (Ref 16). Further, for high-temperature applications requiring wear resistance, thermally sprayed (Cr_xC_y-NiCr) coatings are used in light of the excellent corrosion and oxidation resistance of the Ni-Cr alloy and reasonable wear resistance of chromium carbides at temperatures up to 900 °C (Ref 17, 18). The largely used nickel-base powder belongs to the Ni-B-Si system, with the addition of other alloying elements (Ref 19, 20). Cobalt-base alloy containing chromium (Cr), tungsten (W), and carbon (C), known as Stellite-6 has high hardness and has corrosion and wear resistance at higher temperatures (Ref 21, 22).

Vanadium (V), sulfur (S), and sodium (Na) are common impurities in the low-grade petroleum fuels. Molten sulfate-vanadate deposits resulting from the condensation of combustion products of such fuels are extremely corrosive to high-temperature materials in the combustion systems (Ref 23). Further, mixture of Na_2SO_4 and V_2O_5 in the ratio of 40:60 constitutes eutectics with a low melting point of 550 °C and provides a very aggressive environment for hot corrosion to occur (Ref 24). Cyclic study of 50 cycles (cycle of 1 h heating and 20 min cooling) is considered adequate (Ref 25-27). It provides the severest conditions for testing and may represent the actual industrial environment where breakdown/shutdown occurs frequently. Cyclic study of the candidate HVOF coatings in the given molten salt environment has not been available in the open literature.

So the objective of this study is to evaluate the corrosion resistance of HVOF sprayed Cr_3C_2-NiCr, NiCrBSi, Ni-20Cr, and Stellite-6 coatings on a nickel-base superalloy namely Superni 601 (similar grade Inconel 601) in an aggressive environment of molten salt Na_2SO_4-60%V_2O_5 (wt.%) at 900 °C under cyclic conditions. The substrate superalloy has been provided by Mishra Dhatu Nigam Limited, Hyderabad (India), to find suitable protective coatings to prolong the lifetime of the superalloy for using it at higher temperatures in the corrosive environments.

The thermogravimetric technique was used to establish kinetics of corrosion. X-ray diffraction (XRD), scanning electron microscopy/electron dispersive analysis by x-ray (SEM/EDAX), and electron probe microanalysis (EPMA) techniques have been used to characterize the coatings and corrosion products after hot corrosion at 900 °C.

Table 1 Composition of the coating alloys

Coating alloys	Chemical composition, wt.%	Particle size	Shape
Cr_3C_2-NiCr powder (LA-6875)	75 Cr_3C_2-25 (Ni-20Cr)	−45 μm + 5 μm	Irregular
Blend of 75% LA-6304 and 25% LA-7319	…	…	…
NiCrBSi powder (PA 101HV)	Ni-15.3Cr-3.1B-4.8Si-4.2Fe-0.6C	−45 μm	Spherical
Stellite-6 powder (Jet-Kote 7206)	Co-1.2C-28Cr-4.9W-2.7Fe-2.3Ni-1.1Si	−45 μm	Spherical
Ni-20Cr wire	Ni-20Cr	Wire diameter, 3.17 mm	…

2. Experimental Procedure

2.1 Development of the Coatings

2.1.1 Substrate Material and Coating Formulation. The substrate material used in the study was nickel-base superalloy Superni 601, which was developed by M/S Mishra Dhantu Nigham Limited, Hyderabad (India). The chemical composition of the substrate material is 62.6Ni-23Cr-1.4Al-0.1Mn-0.37Si-0.10Cu-0.025C-bal Fe. This superalloy is used as a high-temperature heat-resistant alloy. The specimens with dimensions of approximately 20 × 15 × 5 mm were cut from the alloy sheet, polished with SiC papers down to 180 grit, and subsequently grit blasted with alumina powders (grit 45) before spraying of the coatings by HVOF. Specimens were prepared manually, and all care was taken for any structural changes in the specimens.

Four types of commercially available coating alloys—Cr_3C_2-NiCr, NiCrBSi and Stellite-6 in the powder form, and Ni-20Cr in the wire form—were used in the study. Details of these coating alloys are given in Table 1.

Coatings were sprayed at M/S Metallizing Equipment Co. Pvt. Ltd., Jodhpur (India) by using two types of commercial HVOF thermal spray systems: Hipojet-2100 HVOF system for powder spraying and Hijet-9600 HVOF system for wire spraying. The spray parameters used for Hipojet-2100 system were: oxygen flow rate, 250 lpm (liters per minute); fuel ((liquefied petroleum gas [LPG]) flow rate, 60 lpm; airflow rate, 900 lpm; spray distance, about 200 mm; fuel pressure, 6 kg/cm^2; oxygen pressure, 8 kg/cm^2; and air pressure, 6 kg/cm^2. The spray parameters used for Hijet-9600 system were the same except oxygen flow rate was 200 lpm, fuel (LPG) flow rate was 50 lpm, fuel pressure was 4 kg/cm^2, and oxygen pressure was 6 kg/cm^2. The specimens were cooled with compressed air jets during and after spraying.

2.1.2 Measurement of Thickness, Porosity, and Hardness of the As-Sprayed Coatings. The coating thickness was measured by taking backscattered electron images (BSEI) along the cross sections of the specimens with a LEO (Leo Electron Microscopy Ltd., Cambridge, UK) 435VP scanning electron microscope equipped with a Robinson backscattered detector (RBSD). Coated samples were subjected to wheel cloth polishing before measuring the porosity. Porosity measurement was done with the help of an image analyzer having software of Dewinter Material Plus 1.01 based on ASTM B 276 (Ref 28).

The images were obtained through the attached PMP3 Inverted Metallurgical Microscope. The microhardness of coatings was measured by Leitz Hardness Tester Miniload 2 fitted with a Vickers pyramidal diamond indenter. The reported values of hardness represent the average of a minimum of five measurements. A 15 g (147.1 mN) load was provided to the needle for penetration, and hardness value (HV) was based on the relation $HV = 1854.4 \times F/d^2$ (where F is load in grams and d is the mean penetrated diameter in μm).

2.1.3 SEM/EDAX and XRD Analysis. A JEOL (JSM-5800, New York) scanning electron microscope with Oxford (Model-6841, England) EDAX attachment was used for surface SEM/EDAX analysis of the coatings and corrosion products. XRD analysis was done with a Bruker AXS D-8 Advance Diffractometer, with Cu Kα radiation.

2.2 Molten Salt Corrosion Tests

Cyclic studies were performed in molten salt (Na_2SO_4-60wt.%V_2O_5) for 50 cycles. Each cycle consisted of 1 h heating at 900 °C in a silicon carbide tube furnace in open air atmosphere followed by 20 min cooling at room temperature. The studies were performed for uncoated as well as coated specimens for the purpose of comparison. The specimens were mirror polished down to 1 μm alumina wheel cloth polishing before corrosion run. Thereafter, the specimens were washed with acetone and heated in an oven to about 250 °C. The specimens were heated to ensure proper adhesion of the salt layer. A layer of Na_2SO_4-60%V_2O_5 mixture prepared in distilled water was applied uniformly on the warm specimens with the help of a camel-hair brush. The amount of the salt coating was kept in the range of 3.0 to 5.0 mg/cm^2. The salt-coated specimens as well as the alumina boats were then kept in the oven for 3 to 4 h at 100 °C. Then they were again weighed before exposing to hot corrosion tests in the tube furnace. The salt mixture was applied on the surface only once in the beginning of the test, and it was not replenished during the test. During hot corrosion runs, the weight of boats and specimens were measured together at the end of each cycle, with the help of Electronic Balance Machine Model 06,120 (Contech, India) with a sensitivity of 1 mg. The spalled scale was also included at the time of measurements of weight change to determine total rate of corrosion. Efforts were made to formulate the kinetics of corrosion. XRD, SEM/EDAX, and EPMA techniques were used to analyze the corrosion products.

3. Results

3.1 Measurements of Thickness, Microhardness, and Porosity of the As-Sprayed Coatings

The thickness of the coatings has been measured from the BSE images and is found in the range of 250 to 300 μm. The microhardness data of the coatings has been compiled in Fig. 1, which shows the microhardness profiles along the cross section of the coatings as a function of distance from the coating/substrate interface. The coatings should have minimum possible porosities as they are the preferential paths from where the corrosion species can penetrate through the coating to reach the substrate and may cause rapid corrosion attack. Porosity measurements were made for the HVOF sprayed coatings on superalloy Superni 601 and found to be less than 2%.

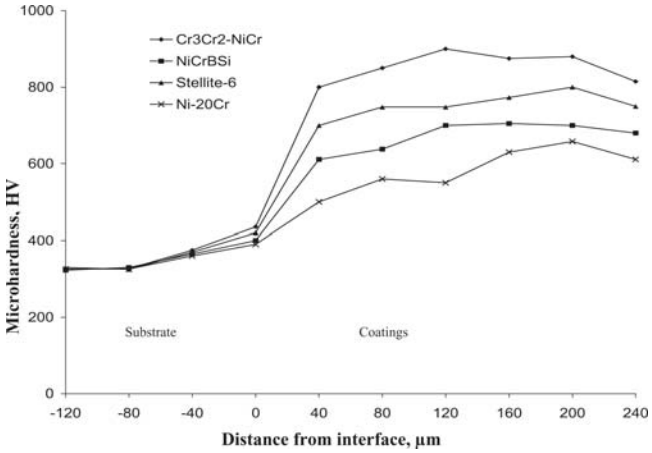

Fig. 1 Microhardness profiles of different HVOF coatings on Superni 601 superalloy along the cross section

3.2 SEM/EDAX and XRD of As-Sprayed Coatings

Scanning electron micrographs showing the surface morphology of the as-sprayed coatings are given in Fig. 2. In general, all the coatings have dense microstructures and are free of cracks. Some unmelted and semimelted particles and pores can be seen in the coatings. In the case of Cr_3C_2-NiCr coating (Fig. 2a), partially melted areas have a composition of 68% Cr and 28% Ni, which is close to powder composition. Melted regions in the coatings are found to be nickel-rich splats. In the case of NiCrBSi coating (Fig. 2b), there are globular melted particles in the matrix of the partially melted layer. These melted particles have nearly the same composition as that of powder. In the case of the partially melted areas, the amount of Ni is slightly less and Si has increased. SEM/EDAX analysis of Stellite-6 coating (Fig. 2c) indicates the presence of melted regular size globules that are cobalt-rich splats surrounded by the partially melted zone having nearly the same composition as that of the matrix. In the case of Ni-20Cr wire coated surface (Fig. 2d), one can see the melted coating having composition similar to the wire, with some partially melted areas where the Ni content is slightly higher, and this region is depleted of Cr. In the micrographs, the regions marked M indicate the melted region, whereas p represents the partially melted/unmelted particles.

EDAX analysis of the Stellite-6 coated superalloys Superfer 800H is shown in Fig. 3. Some contrast stringers at point 4 where EDAX analysis shows the presence of a small quantity of oxygen most likely correspond to the oxide phase. These oxide stringers have appeared in the microstructure in the form of either intersplat lamellae or globules and are oriented parallel to the substrate surface. Some limited oxidation might have occurred at the surface of in-flight particles or at the coating surface, prior to the deposition of the next layer. Black areas at the coating/substrate interface (point 2) might be the inclusions of aluminum oxide, where only aluminum and oxygen are exclusively present. It is believed that some alumina particles might have been retained in the asperities during grit blasting of the substrate prior to deposition of the coatings. Further analysis at point 3 shows that the light gray phase comprises cobalt-rich splats with substantial amounts of Cr.

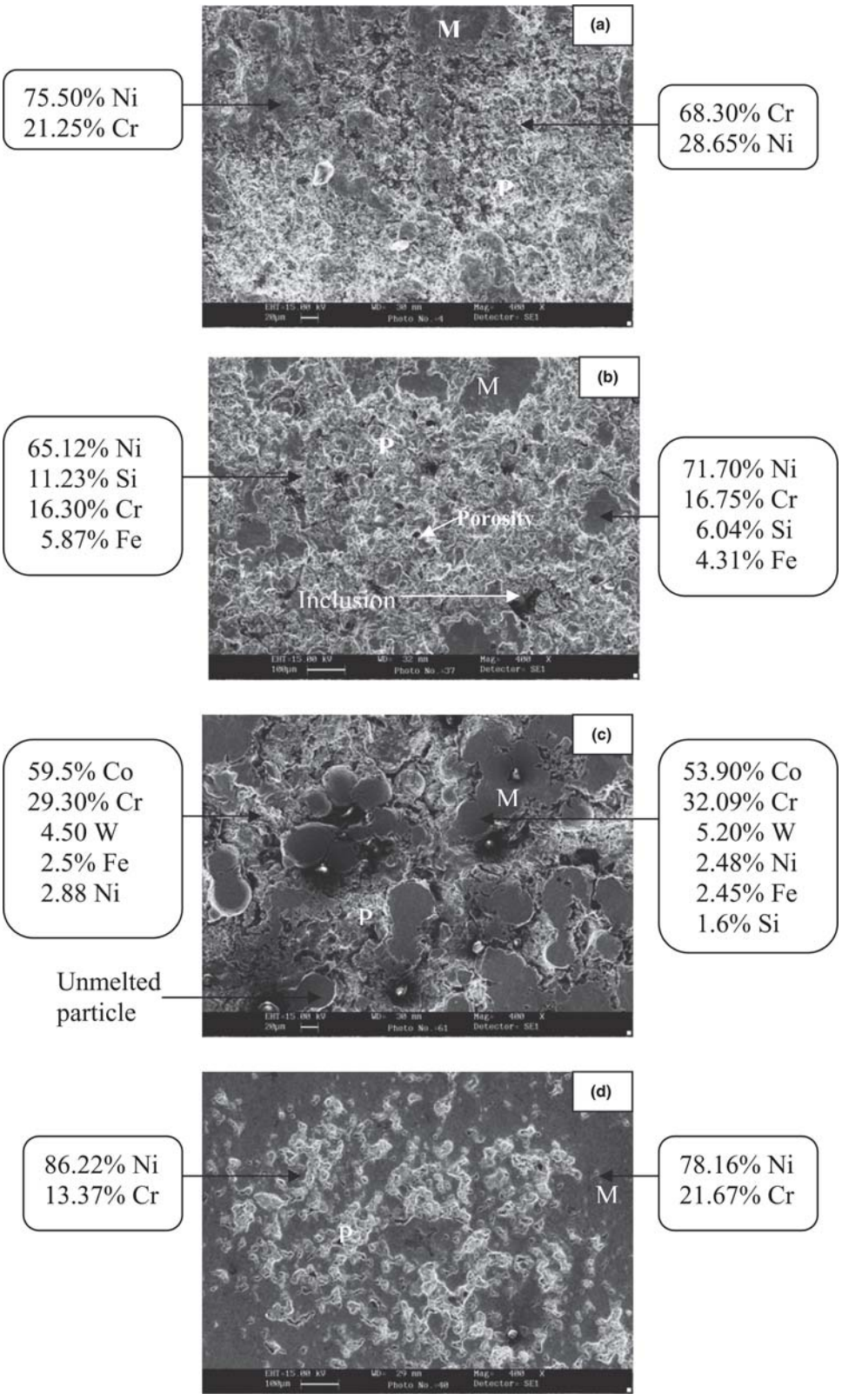

Fig. 2 SEM/EDAX analysis of the as-sprayed coatings on the superalloy Superni 601. Original magnification: 400×. (a) Cr_3C_2-NiCr coating. (b) NiCrBSi coating. (c) Stellite-6 coating. (d) Ni20Cr coating

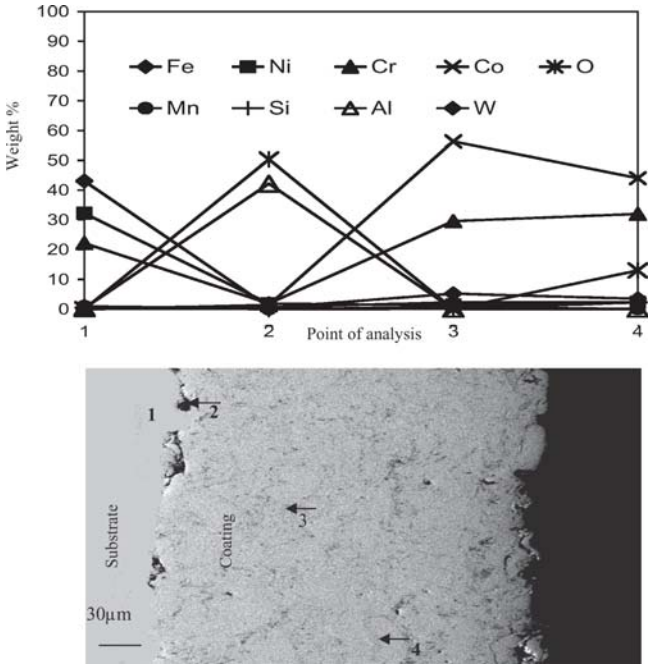

Fig. 3 EDAX analysis across the cross section of the Stellite-6 coating on Superfer 800H

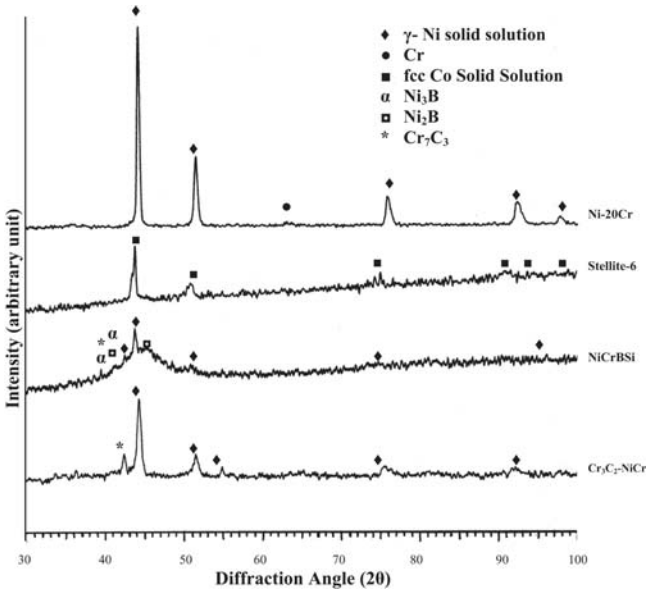

Fig. 4 XRD for the different as-sprayed coatings on Superalloy Superni 601

An x-ray diffractogram is shown in Fig. 4 that indicates that Cr_3C_2-NiCr, NiCrBSi, and Ni-20Cr wire coatings show nickel-base face-centered cubic (fcc) structure as a principal phase, whereas Stellite-6 coating has a principal phase of cobalt-base fcc. In the case of NiCrBSi coatings, the peak around 44° is very broad, suggesting perhaps an amorphous matrix.

3.3 Corrosion Kinetics in Molten Salt

The weight-gain plots for the substrate superalloy hot corroded for 50 cycles with and without coatings, in the presence of a salt layer of Na_2SO_4-60%V_2O_5 at 900 °C, are shown in Fig. 5. The uncoated superalloy shows a subparabolic behavior and a maximum weight gain. Coated superalloy in all the four cases shows a better hot corrosion resistance compared with uncoated superalloy in the given molten salt environment. A fragile scale appeared on the surface of uncoated superalloy during the initial cycles. Subsequently, cracks appeared in the scale, which were confined to the edges. Spalling of the scale was also started from the edges at the end of the fifth cycle. From eighth cycle onward, intensive spalling was observed even from the surface of the superalloy. During the course of study, some of the scale was seen to be detached from the surface of superalloy. The color of the scale, which was brownish gray during early cycles, turned to light gray after some cycles. The surface of the specimen became gradually rough with the progress of study, and an increasing amount of spalled corrosion products could be seen in the boat. The cracks were developed in the scale of uncoated superalloy, as can be seen in Fig. 6.

The Ni-20Cr wire coating has shown a minimum weight gain among all the coatings and has been found to be successful in reducing the weight gain by 75% compared to that for uncoated

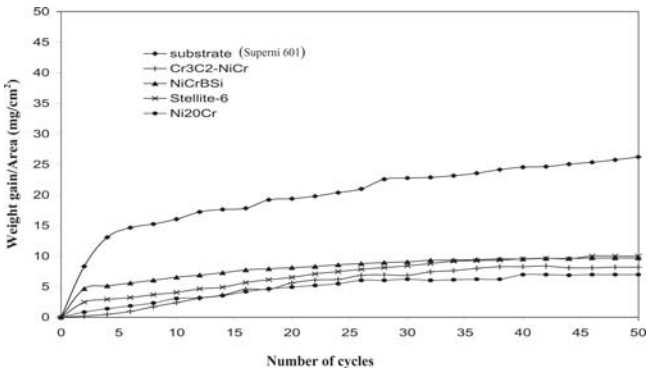

Fig. 5 Weight gain versus number of cycles plot for coated and uncoated superalloy Superni 601 subjected to cyclic oxidation for 50 cycles in Na_2SO_4-60%V_2O_5 at 900 °C

superalloy. Stellite-6 coatings have revealed a relatively higher weight gain that is approximately 1.5 times that gained by Ni-20Cr coatings. However, Stellite-6 coating still shows a tendency to reduce the weight gain by 60% of that gained by the exposed uncoated superalloy. Cr_3C_2-NiCr coating has indicated a second-lowest hot corrosion resistance, followed by NiCrBSi coatings, and they were found to be successful in reducing the weight gain by 68 and 64% of that gained by bare superalloy, respectively. So, all the coatings have shown a tendency to reduce the weight gain by more than 60% of that gained by uncoated superalloy. Figure 7 shows the cumulative weight-gain/unit-area for all the four coatings and substrate superalloy.

The Stellite-6 coated alloy had shown marginal spallation during the tests, whereas spallation was negligible in case of Cr_3C_2-NiCr and Ni-20Cr coated specimens. In the case of Cr_3C_2-NiCr coated alloy, the color of the scale, which was dark gray during earlier cycles, turned to blackish green subsequently. Stellite-6 and Ni-20Cr coated alloy were dark black and

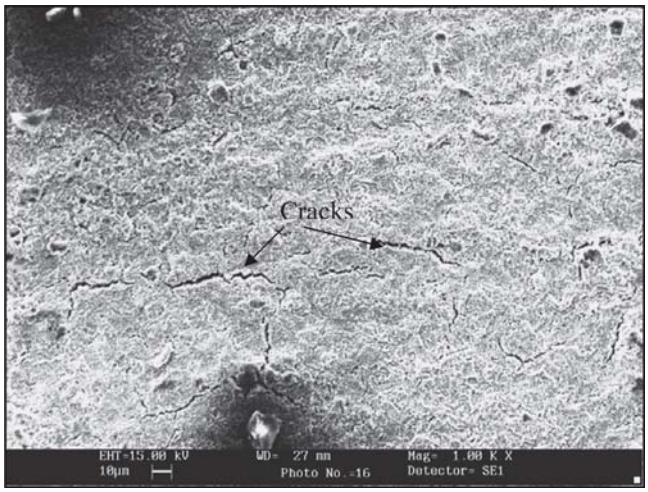

Fig. 6 Cracks developed in the scale of uncoated superalloy Superni 601 subjected to hot corrosion in Na_2SO_4-60%V_2O_5 environment at 900 °C

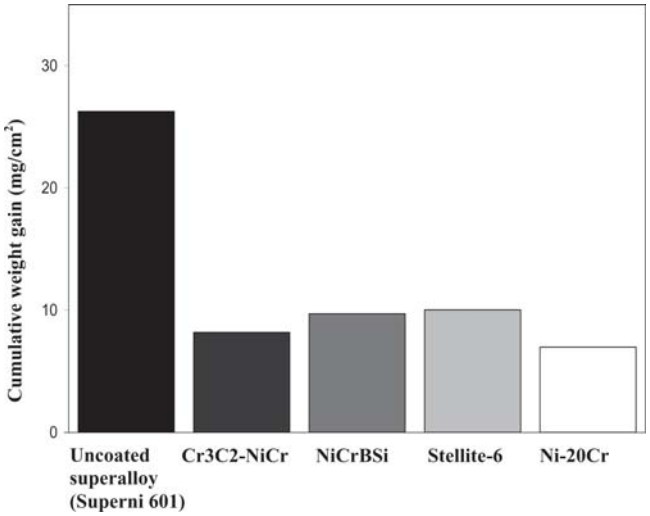

Fig. 7 Bar chart showing cumulative weight gain per unit area for coated and uncoated superalloy Superni 601subjected to cyclic oxidation for 50 cycles in Na_2SO_4-60%V_2O_5 at 900 °C

a shining grayish color, respectively. Rust color compact and dense continuous scale were observed to form on NiCrBSi coated superalloys.

Figure 8 shows (weight gain/area)^2 versus number of cycles plot. It is observed from the graph that all the coatings have followed parabolic rate law; thus they have shown the tendency to act like diffusion barriers to the corroding species. Table 2 shows the values of the parabolic rate constant k_p. The parabolic rate constant k_p was calculated by a linear least-square algorithm to a function in the form of $(\Delta W/A)^2 = k_p \cdot t$, where $\Delta W/A$ is the weight gain per unit surface area (mg/cm^2) and t is the hot corrosion time in seconds.

3.4 SEM/EDAX Analysis of the Scales

Scanning electron micrographs of the substrate and the coated superalloy specimens, showing surface morphology after

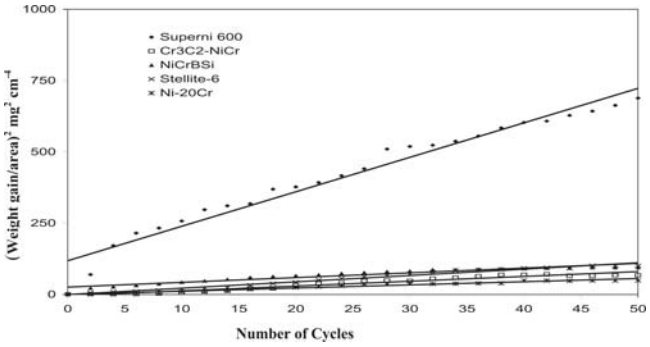

Fig. 8 (Weight gain/area)^2 versus number of cycles plot for coated and uncoated superalloy Superni 601 subjected to cyclic oxidation for 50 cycles in Na_2SO_4-60%V_2O_5 at 900 °C

Table 2 Values of the parabolic rate constant k_p

Description	Parabolic rate constant, k_p, $10^{-10}g^2cm^{-4}s^{-1}$
Uncoated superalloy	33.586
Ni-20Cr coated	3.089
NiCrBSi coated	4.626
Cr_3C_2-NiCr coated	4.703
Stellite-6 coated	6.213

cyclic hot corrosion for 50 cycles at 900 °C, is reported in Fig. 9. The EDAX analysis of the scale for the uncoated specimen showed Fe_2O_3 to be the predominant phase, with substantial amounts of NiO and Cr_2O_3. The scale of the uncoated superalloy shows a rough surface with uniform pitting throughout. The EDAX analysis of Cr_3C_2-NiCr coated specimen shows Cr_2O_3 as the principal phase along with NiO. The scale of NiCrBSi coated superalloy shows nodular appearance with SiO_2 as the predominant phase, and black area in the scale is found to be rich in NiO and Fe_2O_3, whereas Ni-20Cr coating has a fine-grain continuous scale that is mainly Cr_2O_3 and NiO. EDAX analysis of hot corroded Stellite-6 coated superalloy further identified CoO and Cr_2O_3 as main phases and small amounts of NiO, Fe_2O_3, and MnO.

3.5 XRD Analysis

The XRD patterns of the hot corroded specimens after 50 cycles are shown in Fig. 10. It is evident from the diffraction patterns that the corroded uncoated superalloy has shown Fe_2O_3, NiO, $NiCr_2O_4$, and FeV_2O_4 as main phases along with relatively weak peaks of $CrVO_4$. The hot corroded Cr_3C_2-NiCr coated superalloy revealed the presence of Cr_2O_3, NiO, and $NiCr_2O_4$ as main phases with some low-intensity peaks of Fe_2O_3. In addition to these phases, XRD analysis of corroded NiCrBSi coated alloy has also identified SiO_2 as the main phase, whereas Cr_2O_3 phase identified in NiCrBSi coated superalloy has relatively low-intensity peaks as compared with those found in Cr_3C_2-NiCr coated superalloy. The corroded Ni-20Cr coated superalloy has shown the formation of NiO and $NiCr_2O_4$ as main phases along with some weak peaks of Cr_2O_3. In the scale of Stellite-6 coated superalloy, main phases identified are CoO, $CoCr_2O_4$, and $NiCr_2O_4$.

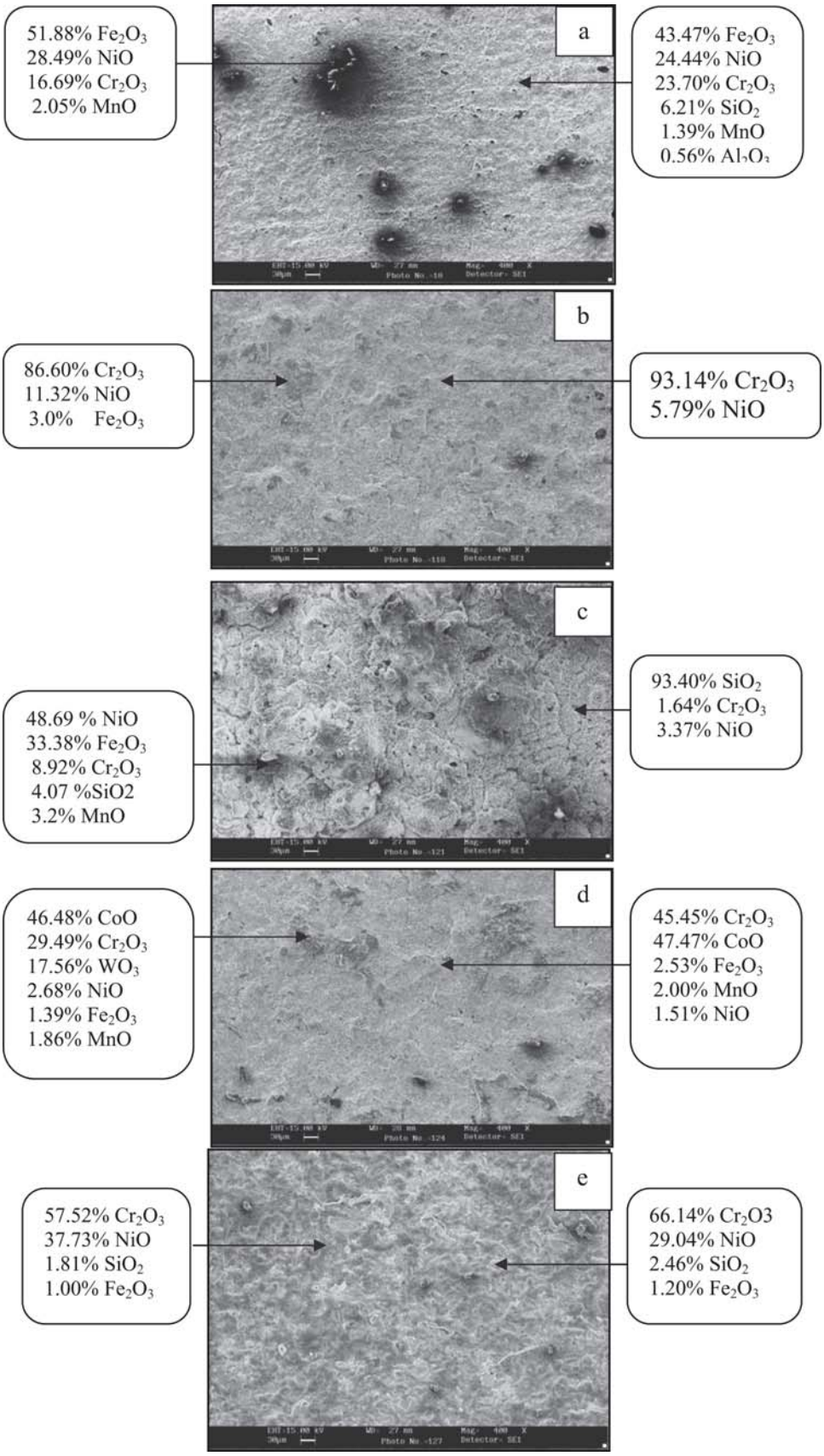

Fig. 9 SEM/EDAX analysis for the superalloy Superni 601 subjected to cyclic oxidation in Na_2SO_4-60%V_2O_5 at 900 °C after 50 cycles. Original magnification: 400×. (a) Uncoated. (b) Cr_3C_2-NiCr coated. (c) NiCrBSi coated. (d) Stellite-6 coated. (e) Ni-20Cr coated

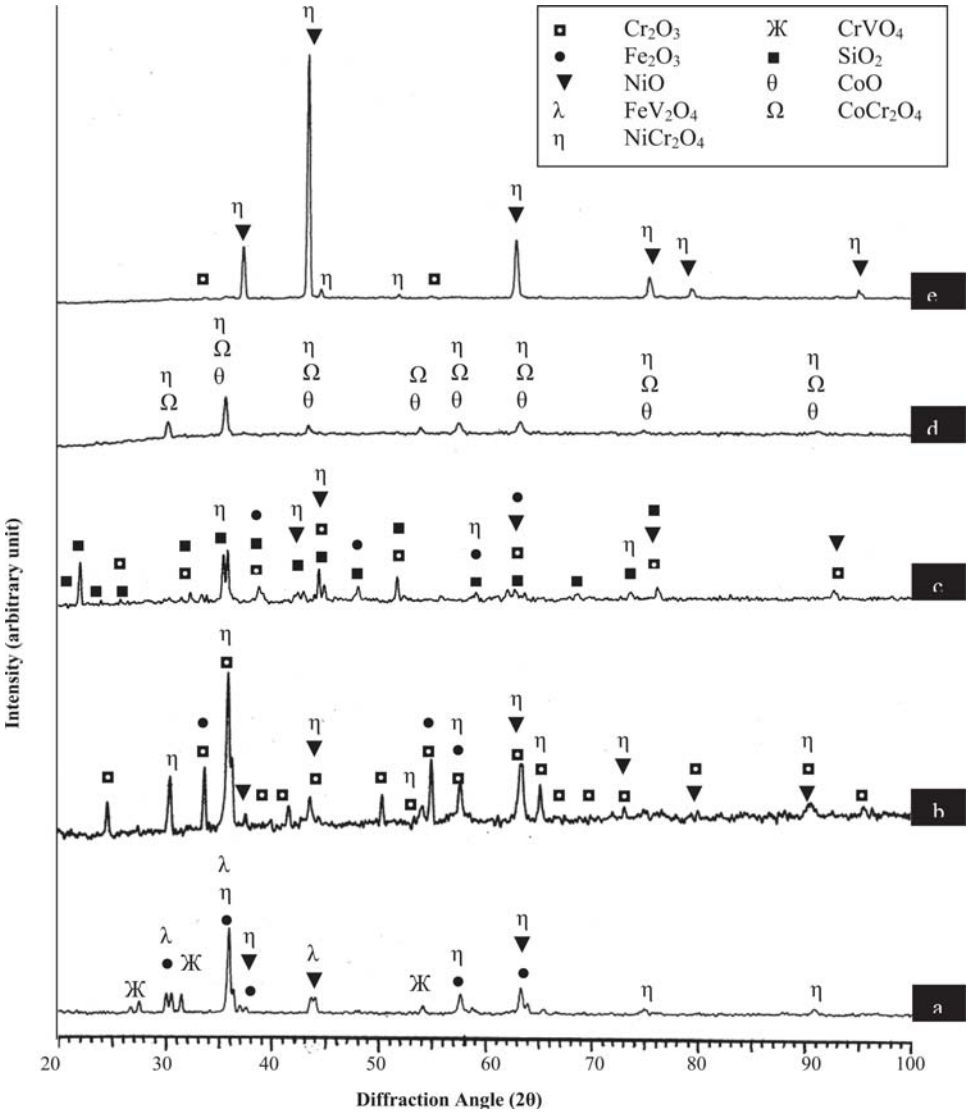

Fig. 10 XRD patterns for the superalloy Superni 601 subjected to cyclic oxidation in Na_2SO_4-60%V_2O_5 at 900 °C after 50 cycles. (a) Uncoated. (b) Cr_3C_2-NiCr coated. (c) NiCrBSi coated. (d) Stellite-6 coated. (e) Ni-20Cr coated

3.6 Cross-Section Analysis of the Oxide Scales

The hot corroded samples were cut across the cross sections and mounted in transoptic mounting resin, mirror polished, and carbon coated to obtain x-ray mapping of the different elements present across the scale.

Elemental x-ray mappings for Cr_3C_2-NiCr coated Superni 601 superalloy (Fig. 11) after hot corrosion in molten salt at 900 °C for 50 cycles show a scale that is mainly rich in Cr and contains Ni also. The coating has retained its lamellar structure, in which nickel-rich splats are present mostly at places that are depleted of Cr. Aluminum and Mn have diffused from the substrate to the coatings along the splat boundaries and also have shown their tendency to form thick and thin streaks at the coating/substrate interface, respectively. Diffusion of iron (Fe) from the substrate to the coating along the splat boundaries is also evident. Silicon has diffused into the entire scale, whereas V and S are present throughout the scale along the splat boundaries, thereby indicating ingress of the same.

X-ray mappings for corroded NiCrBSi coated Superni 601 superalloy are shown in Fig. 12. Micrographs indicate that only the upper part of the coating has oxidized, forming a thick oxide layer consisting of two bands. The topmost band is believed to consist mainly of SiO_2, as Si and oxygen coexist in their respective micrographs. The underlying band appears to consist of unoxidized nickel-rich splats encircled by oxides of mainly Cr and Si. In the underlying band, oxygen is found to be absent where nickel-rich splat are present, whereas at the boundaries of these splats oxygen coexists with Cr and Si. Chromium has shown its tendency to form a thick band in the underlying band just below the topmost band, thereby leaving chromium-depleted band under it. Aluminum coexists with oxygen along the coating/substrate interface, where mostly all other elements are depleted.

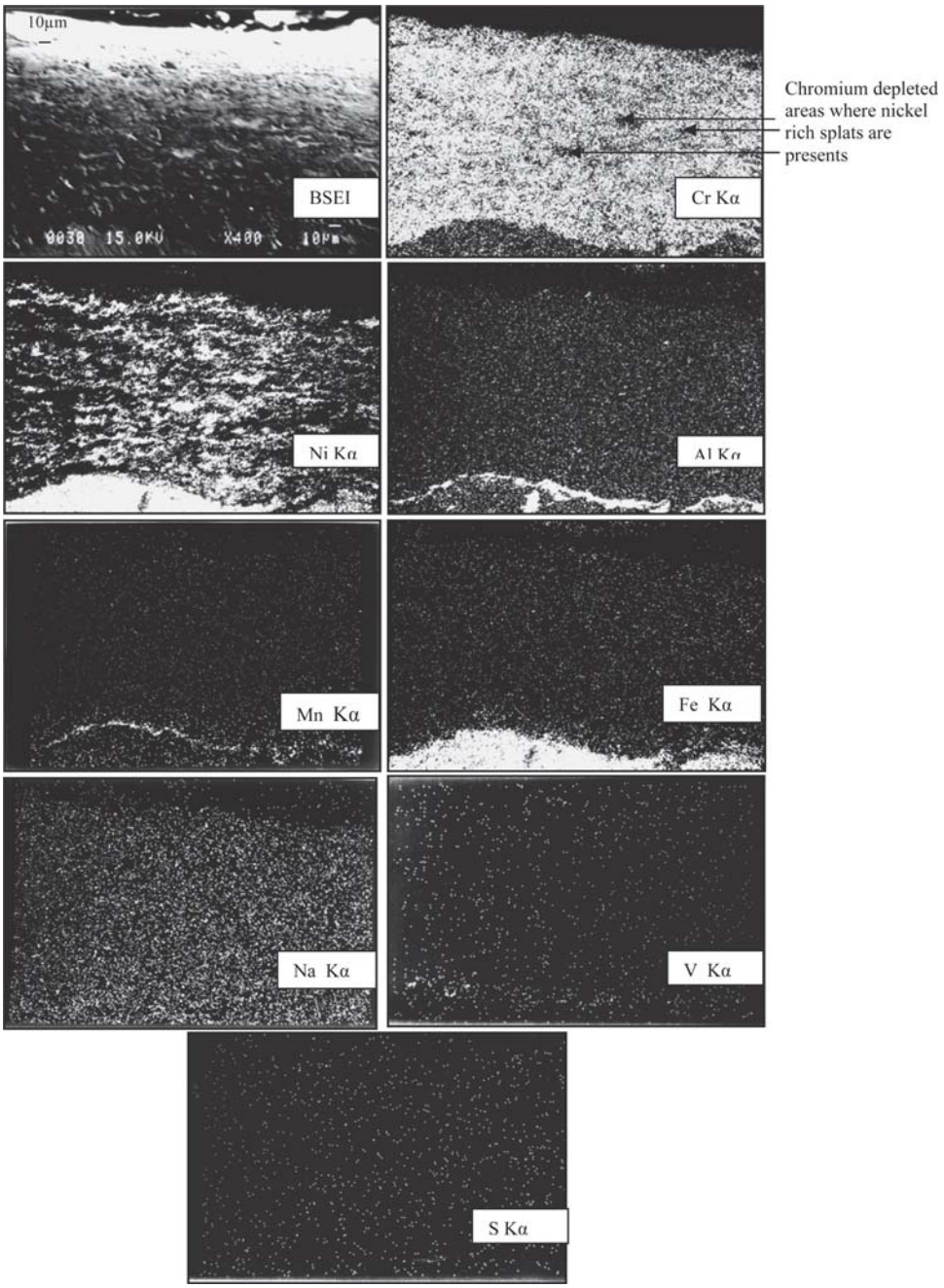

Fig. 11 Composition image (BSEI) and x-ray mapping of the cross section of the Cr_3C_2-NiCr coated superalloy Superni 601 subjected to cyclic oxidation at 900 °C in Na_2SO_4-60%V_2O_5 after 50 cycles

The presence of V, S, and Na below the top scale indicates they have penetrated along the splat boundaries.

Electron probe microanalysis for the cross section of corroded Ni-20Cr coated Superni 601 superalloy indicates the formation of a massive scale mainly consisting of Ni and Cr (Fig. 13). Also present in the scale are Fe, Al, and Si. Nickel-rich splats are present throughout the scale. Aluminum has formed a thick streak at the topmost layer of the scale as well as at the coating/substrate interface, which indicates its tendency to diffuse from the substrate to the coating. There is an underlayer, just below the uppermost layer, mainly rich in Ni and depleted of Cr. Diffusion of Fe into the coating is very intensive near the coating/base-alloy interface. Further, Si and Mn have also migrated into the entire cross section of the scale and have shown their tendency to form small streaks at the splat boundaries.

4. Discussion

Under the spray conditions used for this study, the HVOF process was successfully implemented to develop Cr_3C_2-NiCr,

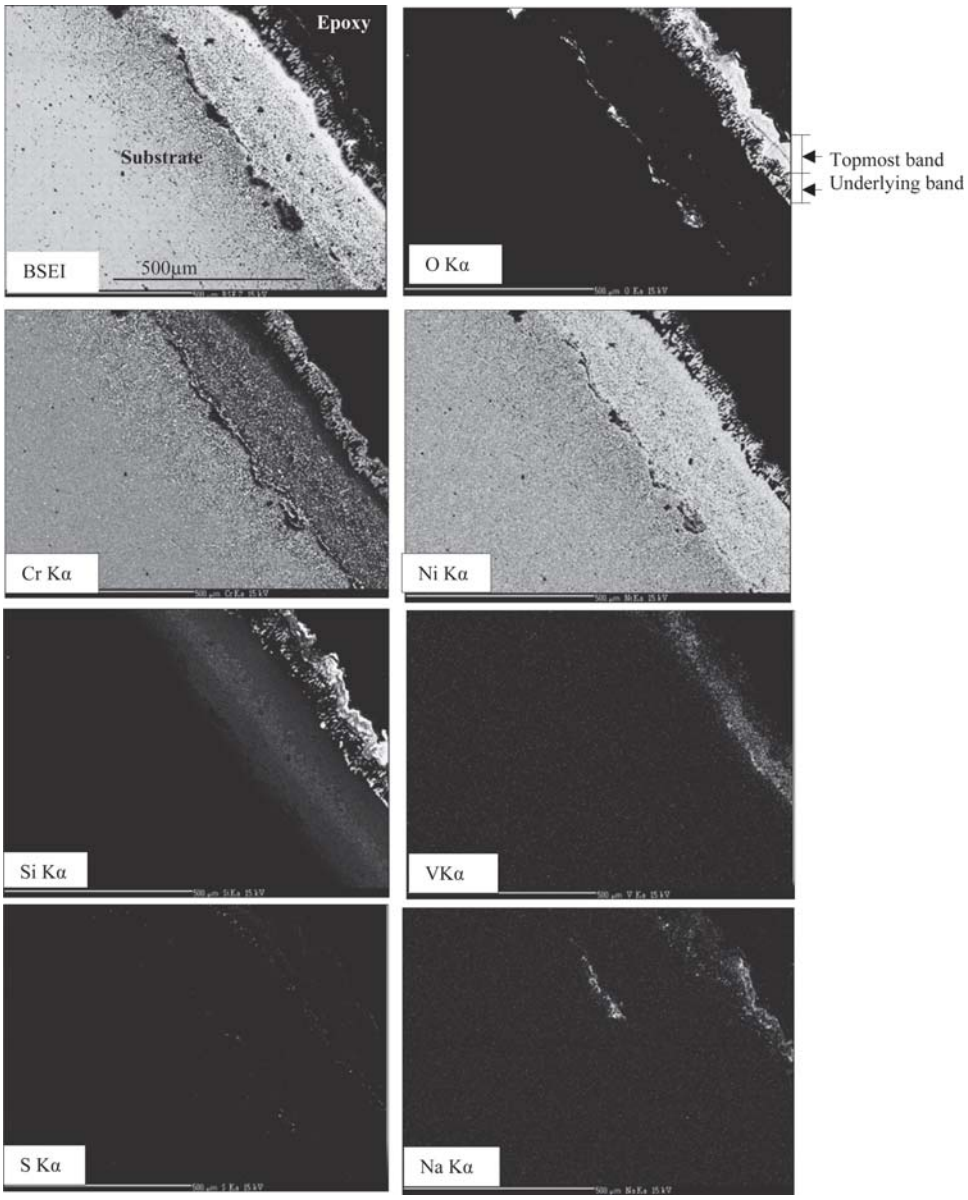

Fig. 12 Composition image (BSEI) and x-ray mapping of the cross section of the NiCrBSi coated superalloy Superfer 601 subjected to cyclic oxidation at 900 °C in Na_2SO_4-60%V_2O_5 after 50 cycles

NiCrBSi, and Stellite-6 powders and Ni-20Cr wire coatings of 250 to 300 μm thick on a nickel-base superalloy Superni 601 with porosity less than 2%. The measured value of porosity is in good agreement with the findings of Miguel et al. (Ref 29), Sahraoui et al. (Ref 30), and Lih et al. (Ref 31). The coating thicknesses, as measured along the cross section for some randomly selected samples, have been found very close to the desired values.

The microhardness of the coatings has been found to be very high as compared with the substrate superalloy (Fig. 1). Further, the substrate near the coating/substrate interface shows a little higher value of hardness compared with the core substrate. This increased hardness value near the coating/substrate interface might be due to the work-hardening effect of sandblasting the substrate prior to the coating process as suggested by Sundararajan et al. (Ref 32). The substrate hardening may also be partly attributed to the high-speed impact of the coating particles during HVOF spraying. Similar phenomenon has also been observed by Sidhu and Prakash (Ref 26) and Hidalgo et al. (Ref 33).

The uncoated specimen indicated accelerated hot corrosion in Na_2SO_4-60%V_2O_5 environment at 900 °C, and the weight gain was enormous as compared with the coated specimens. A very similar weight-change trend had been observed by Gitanjaly (Ref 34) during hot corrosion study for the similar nickel-base superalloy under the same conditions. The weight-gain graph, Fig. 5, shows that the weight increases continuously, although the rate of increase is high during the initial period of exposure. This can mainly be attributed to the formation of $NaVO_3$. At 900 °C, the Na_2SO_4-60%V_2O_5 will combine and

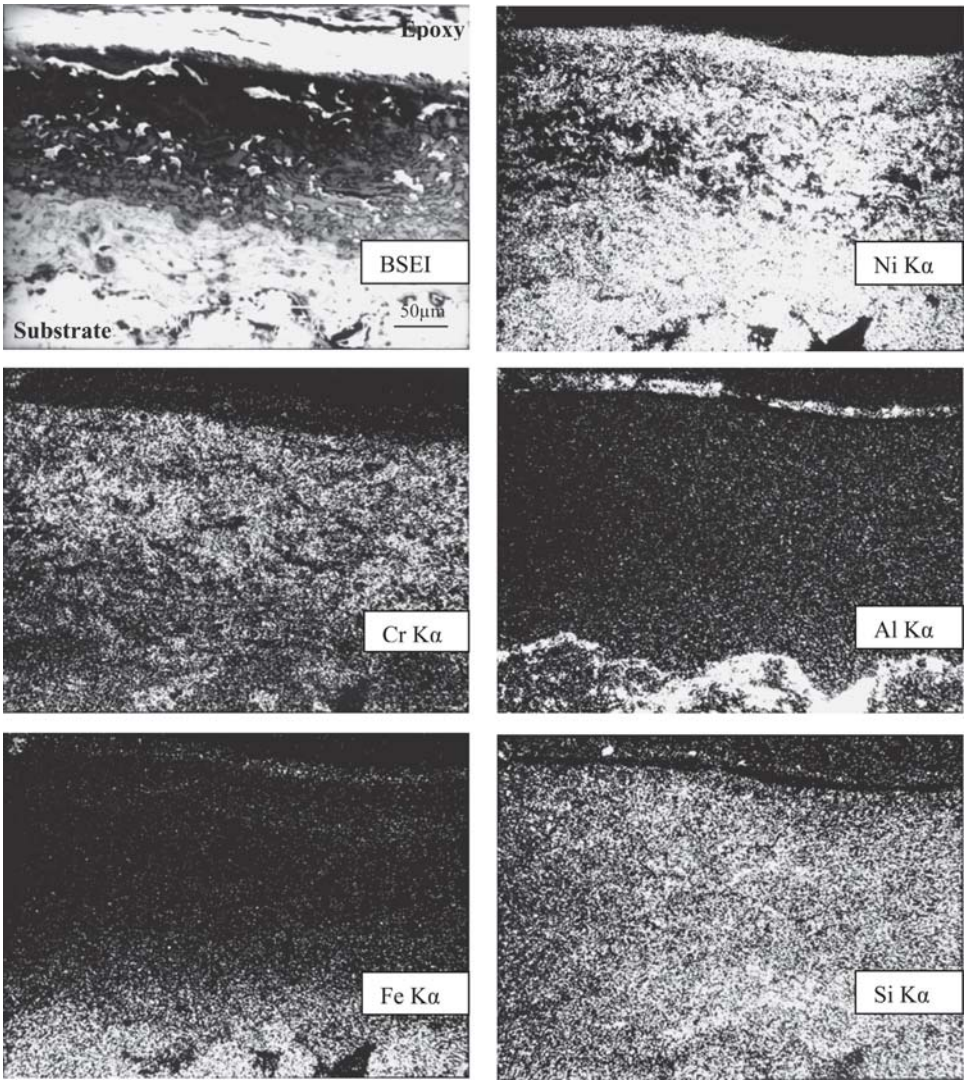

Fig. 13 Composition image (BSEI) and x-ray mapping of the cross section of the Ni-20Cr wire coated superalloy Superfer 601 subjected to cyclic oxidation at 900 °C in Na_2SO_4-60%V_2O_5 after 50 cycles

form $NaVO_3$ having a melting point of 610 °C as proposed by Kolta et al. (Ref 35).

$$Na_2SO_4 + V_2O_5 = 2NaVO_3(l) + SO_2 + \tfrac{1}{2}O_2$$

This $NaVO_3$ acts as a catalyst and also serves as an oxygen carrier to the base alloy, which will lead to the rapid oxidation of the basic elements of the superalloy to form the protective oxide scale. So in the earlier stages of hot corrosion, there is a rapid increase in weight of the uncoated specimen. The rapid increase in weight gain during initial hours was also reported by Gitanjali et al. (Ref 34) and Tiwari et al. (Ref 36) during their studies on the hot corrosion behavior of nickel-base superalloy. Slower increase in weight gain after initial rise is probably caused by the simultaneous growth and dissolution of oxide scale in the molten salt due to the reaction $Cr_2O_3 + 4NaVO_3 + 3/2O_2 \rightarrow 2Na_2CrO_4 + 2\,V_2O_5$ (Ref 37, 38). Fryburg et al. (Ref 39) have suggested that this Na_2CrO_4 gets evaporated as a gas.

The scales formed on the coated specimens were found to be intact with no or very little spallation, whereas intensive spalling of the scale was observed in the case of uncoated specimen. Intensive spalling of the scale of the bare superalloy can be attributed to severe strain developed by the precipitation of Fe_2O_3 from the liquid phase and interdiffusion of intermediate layers of iron oxide as has been reported by Sachs (Ref 40). Further, the presence of different phases in a thin layer might have imposed severe strain on the film, which may result in cracking and exfoliation of the scale. The cracks may have allowed the aggressive liquid phase to reach the metal substrate (Ref 40).

The parabolic rate constant for the uncoated superalloy is found to be greater than the coated superalloy. Further, all the coatings followed a parabolic oxidation behavior up to 50 cycles in the given environment. So it can be inferred that necessary protection has been provided by all the coatings to the substrate.

The formation of oxides along the splat boundaries of the coatings might have acted as a diffusion barrier to the inward diffusion of corrosive species.

Thermal cycles may lead to the spalling/peeling of the oxides formed on the surface of the coatings, especially on the edges and corners of the specimens (Ref 41), which may be attributed to different values of thermal expansion coefficients of the coatings and the substrate as reported by Singh et al. (Ref 27), Niranatlumpong et al. (Ref 42), and Sidhu (Ref 43). In the case of NiCrBSi coated superalloys, spalling/peeling of the oxide scale was not observed. Wang et al. (Ref 41) reported that the addition of Si and boron (B) can promote the formation of continuous and dense scale in the initial corrosion stage and improve the adherence of the outer scale to the coating in the subsequent hot corrosion process. So the behavior of this coating was in good agreement with the findings of Wang et al. (Ref 41), and no spalling or peeling of the scale was observed.

Ni-20Cr coating has provided the best protection to the base alloy as it has decreased the overall weight gain by approximately 75%, which is the maximum among all the coatings. This may be attributed to the presence of protective oxides of Ni and Cr, and their spinels as indicated by the XRD/EDAX analysis. These results are in good agreement with the findings of Singh et al. (Ref 27), Sidhu (Ref 43), Longa-Nava et al. (Ref 44), and Calvarin et al. (Ref 45). Calvarin et al. (Ref 45) have established that the oxide scale formed after high-temperature oxidation of Ni-20Cr foils at 900 °C consists of an outer NiO layer and an intermediate layer composed of oxides rich in Ni and Cr. Formation of small amounts of Fe_2O_3 and SiO_2 as indicated by EDAX may be due to their diffusion from the substrate to the coating, which was also noticed by Singh et al. (Ref 27), Sidhu (Ref 43), and Sundararajan et al. (Ref 46). Diffusion of these elements from the substrate to the coatings may have contributed to the better adhesion of the coatings.

Corrosion resistance of Cr_3C_2-NiCr and NiCrBSi coated alloys could be due to the formation of phases such as Cr_2O_3, NiO, and $NiCr_2O_4$. Additional protective phases of SiO_2 might have contributed to the hot corrosion protective behavior of NiCrBSi coating. The Cr_3C_2-NiCr coated alloy has shown slightly better corrosion resistance than NiCrBSi coated alloy, which most probably is due to the formation of rich chromia scale in the former case as revealed by EDAX/XRD analysis. Electron probe microanalysis also indicates the formation of chromium-rich scale (Fig. 11). However, corrosion resistance of both the coatings has been found to be less than that of Ni-20Cr coated superalloy. Cha et al. (Ref 47) also observed similar ranking at a relatively lower temperature and reported that HVOF sprayed Ni-20Cr coatings have better corrosion resistance at 500 °C in $HCl-H_2O-O_2-N_2$ environment than HVOF sprayed Cr_3C_2-NiCr and NiCrBSi coatings. They further reported that high-temperature corrosion performance of Cr_3C_2-NiCr coatings were slightly better than NiCrBSi coatings. Formation of small amounts of Fe_2O_3, as indicated by XRD/EDAX, may be caused by the diffusion of Fe from the substrate, which was also noticed by Singh (Ref 27), Sidhu (Ref 43), and Sundararajan et al. (Ref 46).

The protection imparted by Stellite-6 coating may be due to the formation of oxides of Cr and Co along with spinels of Co, Cr, or Ni. Luthra (Ref 47) proposed that the formation of spinels might stop the diffusion activities through the cobalt oxide (CoO), which in turn suppresses the further formation of this oxide. He further opined that increases in the growth of $CoCr_2O_4$ and Cr_2O_3 in competition with CoO and Co_3O_4 formation increases the corrosion resistance of alloys. The formation of phases CoO, $CoCr_2O_4$, and Cr_2O_3 revealed by XRD/EDAX is in accordance with the studies of Singh (Ref 27), Sidhu (Ref 43), and Luthra (Ref 48).

5. Conclusions

Under the used HVOF spray conditions, the developed coatings have dense and uniform lamellar microstructure with porosity less than 2%. For this range of porosity and mentioned process parameters, the HVOF sprayed Ni-20Cr wire coatings and Cr_3C_2-NiCr, NiCrBSi, and Stellite-6 powders coatings were found to be very useful in developing the hot corrosion resistance in a nickel-base superalloy, namely Superni 601.

As revealed by XRD analysis, the Cr_3C_2-NiCr, NiCrBSi, and Ni-20Cr wire coatings have nickel-base fcc structure as a principal phase, whereas Stellite-6 coating has principal phase of cobalt-base fcc.

The uncoated superalloy underwent intense spalling and peeling off the scale and the weight gain was enormous during hot corrosion study in the molten salt environment of Na_2SO_4-60%V_2O_5 at 900 °C. Ni-20Cr wire coating has high corrosion resistance and provided the best protection to the base alloy, which may be due to the presence of oxides of nickel and chromium, and their spinels. It was found to be successful in reducing the weight gain by 75% than that for uncoated superalloy.

The hot corrosion resistance shown by Cr_3C_2-NiCr coating is slightly better compared with NiCrBSi coating, whereas hot corrosion resistance of both the coatings have been found to be less than that of Ni-20Cr coating. However, they performed better than Stellite-6 coating. Cr_3C_2-NiCr and NiCrBSi coatings have shown the formation of protective phases such as NiO, Cr_2O_3, and $NiCr_2O_4$. In addition, another protective phase, SiO_2, is formed in NiCrBSi coating.

The Stellite-6 coating has shown relatively the lowest hot corrosion resistance among the coatings studied; still it was successful in reducing the weight by 62%. The protection shown by this coating may be due to the formation of oxides of Co and Cr and spinels of Co, Cr, or Ni.

There was marginal spalling observed in the case of Stellite-6 coated superalloy during hot corrosion studies, whereas it was negligible in the case of Ni-20Cr coated alloy. The spallation and peeling off oxide scale was not observed in the case of NiCrBSi coated superalloy.

Some elements of the substrate such as Fe, Al, Mn, and Si have shown a tendency to diffuse across the coating/substrate interface.

References

1. P.S. Liu, K.M. Liang, and S.R. Gu, High-Temperature Oxidation Behavior of Aluminide Coatings on a New Cobalt-Base Superalloy in Air, *Corros. Sci.,* 2001, **43,** p 1217-1226
2. P.S. Sidky and M.G. Hocking, Review of Inorganic Coatings and Coating Processes for Reducing Wear and Corrosion, *Br. Corros. J.,* 1999, **34**(3), p 171-183
3. W. Brandl, G. Marginean, D. Maghet, and D. Utu, Effects of Specimen

Treatment and Surface Preparation on the Isothermal Oxidation Behaviour of the HVOF-Sprayed MCrAlY Coatings, *Surf. Coat. Technol,* 2004, **188-189,** p 20-26
4. W. Brandl, D. Toma, and H.J. Grabke, The Characteristics of Alumina Scales Formed on HVOF-Sprayed MCrAlY Coatings, *Surf. Coat. Technol.,* 1998, **108-109**(1-3), p 10-15
5. D.W. Parker and G.L. Kutner, HVOF-Spray Technology-Poised for Growth, *J. Adv. Mater. Process.,* 1991, **139**(4), p 68-72, 74
6. *Diamond Jet System and Gun Manual,* Metco/Perkin Elmer, 1989
7. J.M. Guilemany, J. Fernandez, J.M. de Paco, and J. Sanchez, Corrosion Resistance of HVOF WC-Co and TiC/Ni-Ti Coatings Sprayed on Commercial Steel, *J. Surf. Eng.,* 1998, **14**(2), p 133-135
8. A. Collazo, X.R. Novo, and C. Perez, Corrosion Behaviour of Cermet Coatings in Artificial Seawater, *Electrochim. Acta,* 1999, **44**(24), p 4289-4296
9. K. Tani, M. Adachi, A. Nakahira, and Y. Takatani, Aqueous Corrosion Behavior of Thermally Sprayed Coatings for Steel Substrate, *Thermal Spray: Surface Engineering via Applied Research,* C.C. Berndt, Ed., May 8-11, 2000 (Montréal, Québec, Canada), ASM International, 2000, p 1025-1031
10. P. Gu, B. Arsenault, J.J. Beaudoin, J.G. Legoux, B. Harvey, and J. Fournier, Polarization Resistance of Stainless Steel-Coated Rebars, *Cem. Conc. Res.,* 1998, **28**(3), p 321-327
11. A.J. Sturgeon and D.C. Buxton, The Electrochemical Corrosion Behavior of HVOF Sprayed Coatings, *Thermal Spray: Surface Engineering via Applied Research,* C.C. Berndt, Ed., May 8-11, 2000 (Montréal, Québec, Canada), ASM International, 2000, p 1011-1015
12. D. Harvey, O. Lunder, and R. Henriksen, The Development of Corrosion Resistant Coatings by HVOF Spraying, *Thermal Spray: Surface Engineering via Applied Research,* C.C. Berndt, Ed., May 8-11, 2000 (Montréal, Québec, Canada), ASM International, 2000, p 991-997
13. K.S. Tan, J.A. Wharton, and R.J.K. Wood, Solid Particle Erosion-Corrosion Behaviour of a Novel HVOF Nickel Aluminium Bronze Coating for Marine Applications—Correlation between Mass Loss and Electrochemical Measurements, *Wear,* 2005, **258**(1-4), p 629-640
14. M.G. Hocking, Coatings Resistant to Erosive/Corrosive and Severe Environments, *Surf. Coat. Technol.,* 1993, **62**(1-3), p 460-466
15. I. Gurrappa, Identification of Hot Corrosion Resistant MCrAlY Based Bond Coatings for Gas Turbine Engine Applications, *Surf. Coat. Technol,* 2001, **139**(2-3), p 272-283
16. G.W. Goward, Overview: Protective Coatings-Purpose, Role, and Design, *Mater. Sci. Technol.,* 1986, **2,** p 194-200
17. B.Q. Wang and K. Luer, The Erosion-Oxidation Behaviour of HVOF Cr_3C_2-NiCr Cermet Coating, *Wear,* 1994, **174**(1-2), p 177-185
18. J.M. Guilemany, J. Nutting, and N.L. Isern, Microstructural Examination of HVOF Chromium Carbide Coatings for High Temperature, *J. Therm. Spray Technol.,* 1996, **5**(4), p 483-489
19. F. Otsubo, H. Era, and K. Kishitake, Structure and Phases in Nickel-Base Self-Fluxing Alloy Coating Containing High Chromium and Boron, *J. Therm. Spray Technol,* 2000, **9**(1), p 107-113
20. S. Lebaili and S. Hamar-Thibault, Equilibres Liquide-Solide Dans Le Systeme Ni-B-Si Dans la Region Riche en Nickle, *Acta Metall,* 1987, **35**(3), p 701-710, in French
21. K.C. Antony, Wear -Resistant Cobalt-Base Alloys, *J. Met.,* 1983, **35**(2), p 52-60
22. P. Crook, Cobalt and Cobalt Alloys, *Properties and Selection: Nonferrous Alloys and Special-Purpose Materials,* Vol 2, *Metals Handbook,* ASM International, 1991, p 446-454
23. Y.S. Hwang and R.A. Rapp, Thermochemistry and Solubilities of Oxides in Sodium Sulfate-Vanadate Solutions, *Corrosion,* 1989, **45**(11), p 933-937
24. S.N. Tiwari, Ph.D. Thesis, Met. and Mat. Eng. Dept., IIT Roorkee, India, 1997
25. G.C. Wood and T. Hodgkiss, Mechanism of Oxidation of Dilute Nickel-Chromium Alloys, *Nature,* 1996, **211,** p 1358-1361
26. B.S. Sidhu and S. Prakash, Evaluation of the Corrosion Behaviour of Plasma-Sprayed Ni_3Al Coatings on Steel in Oxidation and Molten Salt Environments at 900 °C, *Surf. Coat. Technol.,* 2003, **166,** p 89-100
27. H. Singh, D. Puri, and S. Prakash, Some Studies on Hot Corrosion Performance of Plasma Sprayed Coatings on a Fe-Based Superalloy, *Surf. Coat. Technol,* 2005, **192**(1), p 27-38
28. "Apparent Porosity in Cemented Carbides," B 276, *Annual Book of ASTM Standards,* ASTM, 2005
29. J.M. Miguel, J.M. Guilemany, and S. Vizcaino, Tribological Study of NiCrBSi Coating Obtained by Different Processes, *Tribol. Int.,* 2003, **36**(3), p 181-187
30. T. Sahraoui, N.-E. Fenineche, G. Montavon, and C. Coddet, Structure and Wear Behavior of HVOF Sprayed Cr_3C_2-NiCr and WC-Co Coatings, *Mater. Des.,* 2003, **24**(5), p 309-313
31. W.-C. Lih, S.H. Yang, C.Y. Su, S.C. Huang, I.C. Hsu, and M.S. Leu, Effects of Process Parameters on Molten Particle Speed and Surface Temperature and the Properties of HVOF CrC/NiCr Coatings, *Surf. Coat. Technol.,* 2000, **133-134,** p 54-60
32. T. Sundararajan, S. Kuroda, and A. Fujio, Steam Oxidation Studies on 50Ni-50Cr HVOF Coatings on 9Cr-1Mo Steel: Change in Structure and Morphology across the Coating/Substrate Interface, *Mater. Trans.,* 2004, **45**(4), p 1299-1305
33. V.H. Hidalgo, J.B. Varela, J.M. Calle, and A.C. Menendez, Characterisation of NiCr Flame and Plasma Sprayed Coatings for Use in High Temperature Regions of Boilers, *Surface Eng.,* 2000, **16**(2), p 137-142
34. Gitanjaly, Ph.D. Thesis, Met. & Mat. Eng. Dept., IITR, Roorkee, India, 2003
35. G.A. Kolta, I.F. Hewaidy, and N.S. Felix, Reactions between Sodium Sulphate and Vanadium Pentoxide, *Thermochim. Acta,* 1972, **4,** p 151-164
36. S.N. Tiwari and S. Prakash, Studies on the Hot Corrosion Behaviour of Some Superalloys in Na_2SO_4-V_2O_5, paper C33, Symposium on Localised Corrosion and Environmental Cracking (SOLCEC) (Kalpakkam, India), Jan 22-24 1997
37. M. Seiersten and P. Kofstad, The Effect of SO_3 on Vanadate-Induced Hot Corrosion, *High Temp. Technol.,* 1987, **5**(3), p 115-122
38. J. Swaminathan, S. Raghavan, and S.R. Lyer, Studies on the Hot Corrosion of Some Nickel-Base Superalloys by Vanadium Pentoxide, *T. Indian I, Metals,* 1993, **46**(3), p 175-181
39. G.C. Fryburg, F.J. Kohl, and C.A. Stearns, Chemical Reactions Involved in the Initiation of Hot Corrosion of IN-738, *J. Electrochem. Soc.,* 1984, **131**(12), p 2985-2997
40. K. Sachs, Accelerated High Temperature Oxidation due to Vanadium Pentoxide, *Metallurgia,* April 1958, p 167-173
41. Q.M. Wang, Y.N. Wu, P.L. Ke, H.T. Cao, J. Gong, C. Sun, and L.S. Wen, Hot Corrosion Behavior of AIP NiCoCrAlY(SiB) Coatings on Nickel Base Superalloys, *Surf. Coat. Technol.,* 2004, **186**(3), p 389-397
42. P. Niranatlumpong, C.B. Ponton, and H.E. Evans, The Failure of Protective Oxides on Plasma-Sprayed NiCrAlY Overlay Coatings, *Oxid. Met,* 2000, **53**(3-4), p 241-258
43. B.S. Sidhu, Ph.D. Thesis, Met. & Mat. Eng. Dept., IITR, Roorkee, India, 2003
44. Y. Longa-Nava, Y.S. Yang, M. Takemoto, and R.A. Rapp, Hot Corrosion of Nickel-Chromium and Nickel-Chromium-Aluminum Thermal-Spray Coatings by Sodium Sulfate-Sodium Metavanadate Salt, *Corrosion,* 1996, **52**(9), p 680-689
45. G. Calvarin, R. Molins, and A.M. Huntz, Oxidation Mechanism of Ni-20Cr Foils and its Relation to the Oxide-Scale Microstructure, *Oxid. Met,* 2000, **53**(1-2), p 25-48
46. T. Sundararajan, S. Kuroda, K. Nishida, T. Itagaki, and F. Abe, Behaviour of Mn and Si in the Spray Powders during Steam Oxidation of Ni-Cr Thermal Spray Coatings, *ISIJ Int.,* 2004, **44**(1), p 139-144
47. S.C. Cha, H.W. Gudenau, and G.T. Bayer, Comparison of Corrosion Behaviour of Thermal Sprayed and Diffusion-Coated Materials, *Mater. Corros.,* 2002, **53,** p 195-205
48. K.L. Luthra, Kinetics of the Low Temperature Hot Corrosion of Co-Cr-Al Alloys, *J. Electrochem. Soc.,* 1985, **132**(6), p 1293-1298